Numerical evidence for a small-scale dynamo approaching solar magnetic Prandtl numbers

Jörn Warnecke [1] ✉, Maarit J. Korpi-Lagg [1,2,3], Frederick A. Gent [2,4] & Matthias Rheinhardt [2]

Magnetic fields on small scales are ubiquitous in the Universe. Although they can often be observed in detail, their generation mechanisms are not fully understood. One possibility is the so-called small-scale dynamo (SSD). Prevailing numerical evidence, however, appears to indicate that an SSD is unlikely to exist at very low magnetic Prandtl numbers (Pr_M) such as those that are present in the Sun and other cool stars. Here we have performed high-resolution simulations of isothermal forced turbulence using the lowest Pr_M values achieved so far. Contrary to earlier findings, the SSD not only turns out to be possible for Pr_M down to 0.0031 but also becomes increasingly easier to excite for Pr_M below about 0.05. We relate this behaviour to the known hydrodynamic phenomenon referred to as the bottleneck effect. Extrapolating our results to solar values of Pr_M indicates that an SSD would be possible under such conditions.

Astrophysical flows are considered to be susceptible to two types of dynamo instability. First, a large-scale dynamo (LSD) is excited by flows exhibiting helicity, or more generally, lacking mirror symmetry, due to rotation, shear and/or stratification. It generates coherent, dynamically relevant magnetic fields on the global scales of the object in question[1]. The characteristics of LSDs vary depending on the dominating generative effects, such as differential rotation in the case of the Sun. Convective turbulence provides both generative and dissipative effects[2], and their presence and astrophysical relevance is no longer strongly debated.

The presence of the other type of dynamo instability, namely the small-scale or fluctuation dynamo (SSD), however, remains controversial in solar and stellar physics. In an SSD-active system, the magnetic field is generated at scales comparable to or smaller than the characteristic scales of the turbulent flow, enabled by chaotic stretching of field lines at high magnetic Reynolds number[3]. In contrast to the LSD, excitation of an SSD requires markedly stronger turbulence[1]. Furthermore, it has been theorized that it becomes increasingly more difficult to excite an SSD at very low magnetic Prandtl number Pr_M (refs. 4–10),

the ratio of kinematic viscosity ν and magnetic diffusivity η. In the Sun, Pr_M can reach values as low as 10^{-6}–10^{-4} (ref. 11), thus seriously repudiating whether an SSD can at all be present. Numerical models of SSDs in near-surface solar convection typically operate at $Pr_M \approx 1$ (refs. 12–18) and thus circumvent the issue of low-Pr_M dynamos.

A powerful SSD may potentially have a large impact on the dynamical processes in the Sun. It can, for example, influence the angular momentum transport and therefore the generation of differential rotation[19,20], interact with the LSD[21–25] or contribute to coronal heating via enhanced photospheric Poynting flux[26]. Hence, it is of great importance to clarify whether or not an SSD can exist in the Sun. Observationally, it is still debated whether the small-scale magnetic field on the surface of the Sun has contributions from the SSD or is solely due to the tangling of the large-scale magnetic field by the turbulent motions[27–32]. However, these studies show a slight preference of the small-scale fields to be cycle independent. SSDs at small Pr_M are also important for the interiors of planets and for liquid-metal experiments[33].

Various numerical studies have reported increasing difficulties in exciting the SSD when decreasing Pr_M (refs. 6,10,34), confirming the

theoretical predictions. However, current numerical models reach only $Pr_M = 0.03$ using explicit physical diffusion or slightly lower (estimated) Pr_M, relying on artificial hyperdiffusion[7,8]. To achieve even lower Pr_M, one needs to increase the grid resolution massively (see also ref. [35]). Exciting the SSD requires a magnetic Reynolds number (Re_M) typically larger than 100; hence, for example, $Pr_M = 0.01$ implies a fluid Reynolds number $Re = 10^4$, where $Re = u_{rms}\ell/\nu$, with u_{rms} being the volume integrated root-mean-squared velocity, ℓ a characteristic scale of the velocity and $Re_M = Pr_M Re$. In this Article, we take this path and lower Pr_M substantially using high-resolution simulations.

Results

We include simulations with resolutions of 256^3 to $4,608^3$ grid points and $Re = 46$ to $Re = 33,000$. This allows us to explore the parameter space from $Pr_M = 1$ to $Pr_M = 0.0025$, which is closer to the solar value than has been investigated in previous studies. For each run, we measure the growth rate λ of the magnetic field in its kinematic stage and determine whether or not an SSD is being excited.

To afford an in-depth exploration of the effect of Pr_M, we omit large-scale effects such as stratification, rotation and shear. We avoid the excessive integration times, required to simulate convection, by driving the turbulent flow explicitly under isothermal conditions. Our simulation set-up consists of a fully periodic box with a random volume force (see Methods for details); the flow exhibits a Mach number of around 0.08. In Fig. 1, we visualize the velocity and magnetic fields of one of the highest-resolution and -Reynolds-number cases. As might be anticipated for low-Pr_M turbulence, the flow exhibits much finer, fractal-like structures than the magnetic field. Note that all our results refer to the kinematic stage of the SSD, where the magnetic field strength is far too weak to influence the flow but otherwise arbitrary.

Growth rates and critical magnetic Reynolds numbers

In Fig. 2, we visualize the growth rate λ as function of Re and Re_M. We find positive growth rates for all sets of runs with constant Pr_M if Re_M is large enough. λ increases always with increasing Re_M as expected. Surprisingly, the growth rates are distinctly lower within the interval from $Re = 2,000$ to $Re = 10,000$ than below and above. With the Re_M values used, this maps roughly to a Pr_M interval from about 0.1 to 0.04.

The growth rates for $Pr_M = 0.1$ match very well the ones from ref. [10], indicated by triangles in Fig. 2. From Fig. 2, we clearly see that the critical magnetic Reynolds number Re_M^{crit}, defined by growth rate $\lambda = 0$, first rises as a function of Re and then falls for $Re > 3 \times 10^3$ (see the thin black line). Looking at Re_M^{crit} as a function of magnetic Prandtl number Pr_M, it first increases with decreasing Pr_M and then decreases for $Pr_M < 0.05$. Hence, an SSD is easier to excite here than for $0.05 < Pr_M < 0.1$. We could even find a nearly marginal, positive growth rate for $Pr_M = 0.003125$. The decrease of λ at low Pr_M is an important result as the SSD was believed to be even harder[4,9] or at least equally hard[7,8] to excite when Pr_M was decreased further from previously investigated values. The growth rates agree qualitatively with the earlier work at low Pr_M (refs. [6–8]).

For a more accurate determination of Re_M^{crit}, we next plot the growth rates for fixed Pr_M as a function of Re_M (Fig. 3a). The data are consistent with $\lambda \propto \ln(Re_M/Re_M^{crit})$ as theoretically predicted[36,37]. Fitting accordingly, we are able to determine Re_M^{crit} as a function of Pr_M (Fig. 3b). This plot clearly shows that there are three distinct regions of dynamo excitation. When Pr_M decreases in the range $1 \geq Pr_M \geq 0.1$ it becomes much harder to excite the SSD. In the range $0.1 \geq Pr_M \geq 0.04$, excitation is most difficult with little variation of Re_M^{crit}. For $Pr_M \leq 0.04$, it again becomes easier as Pr_M reduces. In refs. [7,8], the authors already found an indication of Re_M^{crit} to level-off with decreasing Pr_M, however, only when using artificial hyperdiffusion. Similarly, with our error bars, a constant Re_M^{crit} cannot be excluded for $0.01 < Pr_M < 0.1$. However, at $Pr_M = 0.005$, the error bar allows to conclude that Re_M^{crit} is here lower

than at $Pr_M = 0.05$. This again confirms our result that Re_M^{crit} is decreasing with Pr_M for very low Pr_M.

For $Pr_M \leq 0.05$, the decrease of Re_M^{crit} with Pr_M can be well represented by the power law $Re_M^{crit} \propto Pr_M^{0.125}$. Extrapolating this to the Sun and solar-like stars would lead to $Re_M^{crit} \approx 40$ at $Pr_M = 10^{-6}$, which means that we could expect an SSD to be present. For increasing Re, by decreasing ν, it would be reasonable to assert that the statistical properties of the flow and hence Re_M^{crit} become independent of Pr_M. However, episodes of non-monotonic behaviour of Re_M^{crit} when approaching this limit cannot be ruled out.

The well-determined Re_M^{crit} dependency on Pr_M together with its error bars and the power-law fit have been added to Fig. 2, and agree very well with the thin black line for $\lambda = 0$ interpolated from the growth rates.

Regions of dynamo excitation

Next we seek answers to the obvious question arising: why is the SSD harder to excite in a certain intermediate range of Pr_M and easier at lower and higher values? For this, we investigate the kinetic and magnetic energy spectra of a representative subset of the runs (Supplementary Table 2). We show in Fig. 4 the spectra of two exemplary cases: run F005, with $Pr_M = 0.05$, probes the Pr_M interval of impeded dynamo action, while run H0005, with $Pr_M = 0.005$, is clearly outside it (see Supplementary Figs. 1 and 2 for spectra of other cases).

In all cases, the kinetic energy as a function of wavenumber k clearly follows a Kolmogorov cascade with $E_{kin} \propto k^{-5/3}$ in the inertial range. When compensating with $k^{5/3}$, we find the well-known bottleneck effect[38,39]: a local increase in spectral energy, deviating from the power law, as found both in fluid experiments[40–42] and numerical studies[43,44]. It has been postulated to be detrimental to SSD growth[4,10]. For the magnetic spectrum, however, yet clearly visible for only $Pr_M \leq 0.005$, we find a power law following $E_{mag} \propto k^{-3}$. A 3/2 slope at low wavenumbers as predicted by ref. [45] is seen only in the runs with Pr_M close to one, while for the intermediate and low-Pr_M runs, the positive-slope part of the spectrum shrinks to cover only the lowest k values, and the steep negative slopes at high k values become prominent. A steep negative slope in the magnetic power spectra was also seen by ref. [7] for Pr_M slightly below unity. However, the authors propose a tentative power of -1 given that the -3 slope is not yet clearly visible for their Pr_M values.

Analysing our simulations, we adopt the following strategy. For each spectrum, we determine the wavenumber of the bottleneck, k_b, as the location of its maximum in the (smoothed) compensated spectrum, along with its starting point $k_{bs} < k_b$ at the location with 75% of the maximum (Fig. 4, middle). We additionally calculate a characteristic magnetic wavenumber, defined as $k_M = \int_k E_{mag}(k)k\,dk/\int_k E_{mag}(k)\,dk$, which is often connected with the energy-carrying scale. Furthermore, we calculate the viscous dissipation wavenumber $k_\nu = (\epsilon_K/\nu^3)^{1/4}$ following Kolmogorov theory, where ϵ_K is the viscous dissipation rate $2\nu S^2$ with the traceless rate-of-strain tensor of the flow, S. From the relations between these four wavenumbers (listed in Supplementary Table 2), we draw insights about the observed behaviour of Re_M^{crit} with respect to Pr_M.

We plot k_b/k_ν and k_{bs}/k_ν as functions of Pr_M in Fig. 5. As is expected, k_b/k_ν, or the ratio of the viscous scale to the scale of the bottleneck, does not depend on Pr_M, as the bottleneck is a purely hydrodynamic phenomenon. The start of the bottleneck k_{bs} should likewise not depend on Pr_M, but the low Re values for $Pr_M = 1$ to $Pr_M = 0.1$ lead to apparent thinner bottlenecks, hence an unsystematic weak dependency. The red shaded area between k_b and k_{bs} is the low-wavenumber part of the bottleneck where the slope of the spectrum is larger (less negative) than $-5/3$ (see Supplementary Table 2 for values of the modified slope α_b and Supplementary Section 1 for a discussion). We note that $\alpha_b \approx -1.3 \ldots -1.5$ and can thus deviate markedly from $-5/3$. Overplotting the k_M/k_ν curve reveals that it intersects with the red shaded area exactly where the dynamo is hardest to excite (region II). This lets us
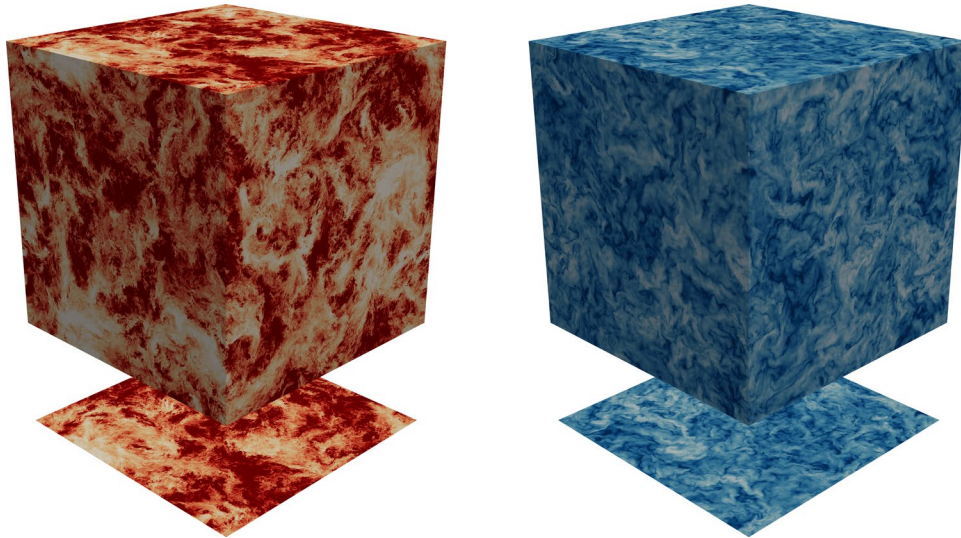
Fig. 1 | Visualization of flow and SSD solution. Flow speed (left) and magnetic field strength (right) from a high-resolution SSD-active run with Re = 18,200 and $Pr_M = 0.01$ on the surface of the simulation box.
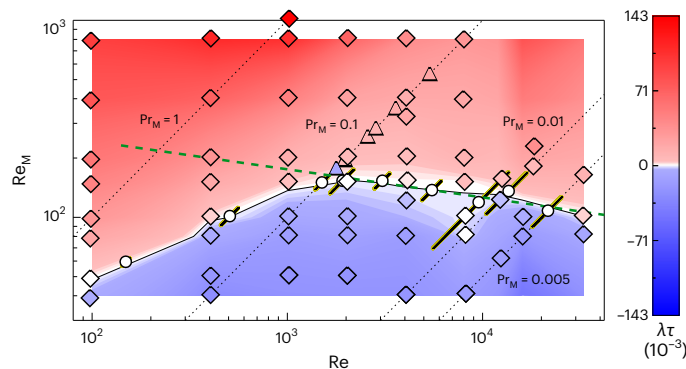

Fig. 2 | SSD growth rate as function of the fluid and magnetic Reynolds numbers (Re and Re_M). The diamonds represent the results of this work and the triangles represent the results of ref. [10]. The colour coding indicates the value of the normalized growth rate $\lambda\tau$ with $\tau = 1/u_{rms}k_f$, a rough estimate for the turnover time. The dotted lines indicate constant magnetic Prandtl number Pr_M. The white circles indicate zero growth rate for certain Pr_M, obtained from fitting for the critical magnetic Reynolds number, as shown in Fig. 3; fitting errors are signified by yellow-black bars (Supplementary Section 5). The background colours, including the thin black line (zero growth), are assigned via linear interpolation of the simulation data. The green dashed line shows the power-law fit of the critical Re_M for $Pr_M \leq 0.08$, with power 0.125 (Fig. 3b).

conclude that the shallower slope of the low-wavenumber part of the bottleneck may indeed be responsible for enhancing Re_M^{crit} in the interval $0.04 \lesssim Pr_M \lesssim 0.1$. Using this plot, we can now clearly explain the three regions of dynamo excitation. For $0.1 \lesssim Pr_M \lesssim 1$ the low-wavenumber part of the bottleneck and the characteristic magnetic scale are completely decoupled. This makes the SSD easy to excite (region I). For $0.04 \lesssim Pr_M \lesssim 0.1$, (grey, region II), the dynamo is hardest to excite because of the shallower slope of the kinetic spectra. In region III, where $Pr_M \lesssim 0.04$ the low-wavenumber part of the bottleneck and the characteristic magnetic scale are again completely decoupled making the dynamo easier to excite.

Further, we find that the dependence of k_M/k_v on Pr_M also differs between the regions. In region I, k_M/k_v depends on Pr_M via $k_M/k_v \propto Pr_M^{0.54}$ and in region II and III via $k_M/k_v \propto Pr_M^{0.71}$. This becomes particularly

interesting when comparing the characteristic magnetic wavenumber k_M with the ohmic dissipation wavenumber which is defined as $k_\eta = k_v Pr_M^{3/4}$. In region I, we find a notable difference of k_M and k_η in value and scaling. However, in region III, the scaling of k_M comes very close to the 3/4 scaling of k_η. This behaviour can be even better seen in the inset of Fig. 5, where the ratio k_M/k_η is 0.3 for $Pr_M = 1$ and tends towards unity for decreasing Pr_M, but is likely to saturate below 0.75.

Discussion

In conclusion, we find that the SSD is progressively easier to excite for magnetic Prandtl numbers below 0.04, in contrast to earlier findings, and thus is very likely to exist in the Sun and other cool stars. Provided saturation at sufficiently high levels, the SSD has been proposed to strongly influence the dynamics of solar-like stars: previous numerical studies, albeit at $Pr_M \approx 1$, indicate that this influence concerns, for example, the angular momentum transport[19,20] and the LSD[21–25]. Our kinematic study, however, only shows that a positive growth rate is possible at very low Pr_M, but not whether an SSD is able to generate dynamically important field strengths. As the Re_M of the Sun and solar-like stars is several orders of magnitude higher than the extrapolated Re_M^{crit} value of 40, we yet expect dynamically important SSDs as indicated by $Pr_M = 1$ simulations[15]. However, numerical simulations with Pr_M down to 0.01 show a decrease of the saturation strength with decreasing Pr_M (ref. [46]).

The results of our study are well in agreement with previous numerical studies considering partly overlapping Pr_M ranges[6–8,10]. Those studies found some discrepancies with the Kazantsev theory[45] for low Pr_M, for example, the narrowing down of the positive Kazantsev spectrum at low and intermediate wavenumbers, and the emergence of a negative slope instead at large wavenumbers[7]. We could extend this regime to even lower Pr_M and therefore study these discrepancies further. For $Pr_M \leq 0.005$, we find that the magnetic spectrum shows a power-law scaling k^{-3}, which is substantially steeper than the tentative k^{-1} one proposed in ref. [7] for $0.03 \lesssim Pr_M \lesssim 0.07$ (but only for eighth-order hyperdiffusivity). This finding of such a steep power law in the magnetic spectrum challenges the current theoretical predictions and might indicate that the SSD operating at low Pr_M is fundamentally different from that at $Pr_M \approx 1$.

Second, we find that the growth rates near the onset follow an $\ln(Re_M)$ dependence as predicted by refs. [36,37], and not a $Re_M^{1/2}$ one as would result from intertial-range-driven SSDs[1,7]. We do not observe a tendency of the growth rate to become independent of Re_M at the
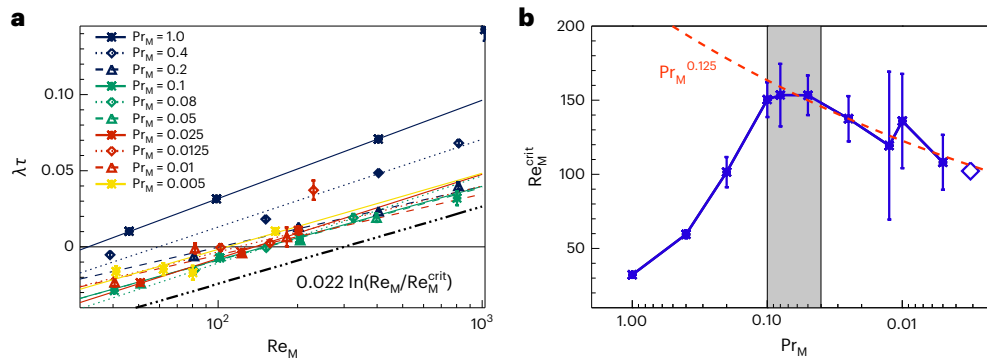
Fig. 3 | Growth rate and critical Reynolds number. a, Normalized growth rate $\lambda\tau$ as function of magnetic Reynolds number Re_M for simulation sets with fixed magnetic Prandtl number Pr_M, indicated by different colours. Logarithmic functions $\lambda\tau \propto \ln(Re_M/Re_M^{crit})$ according to refs. [36],[37] were fitted separately to the individual sets, as indicated by the coloured lines (see the dashed-dotted line for the mean slope). **b**, Critical magnetic Reynolds number Re_M^{crit} as function of

Pr_M obtained from the fits in **a**. The error bars show the fitting error (Supplementary Section 5). The diamond indicates a run with growth rate $\lambda \approx 0$; hence, its Re_M represents $\sim Re_M^{crit}$ for the used $Pr_M = 0.003125$. The red dashed line is a power-law fit $Re_M^{crit} \propto Pr_M^{0.125}$, valid for $Pr_M \lesssim 0.08$. The grey shaded area indicates the Pr_M interval where the dynamo is hardest to excite ($Re_M^{crit} \gtrsim 150$).
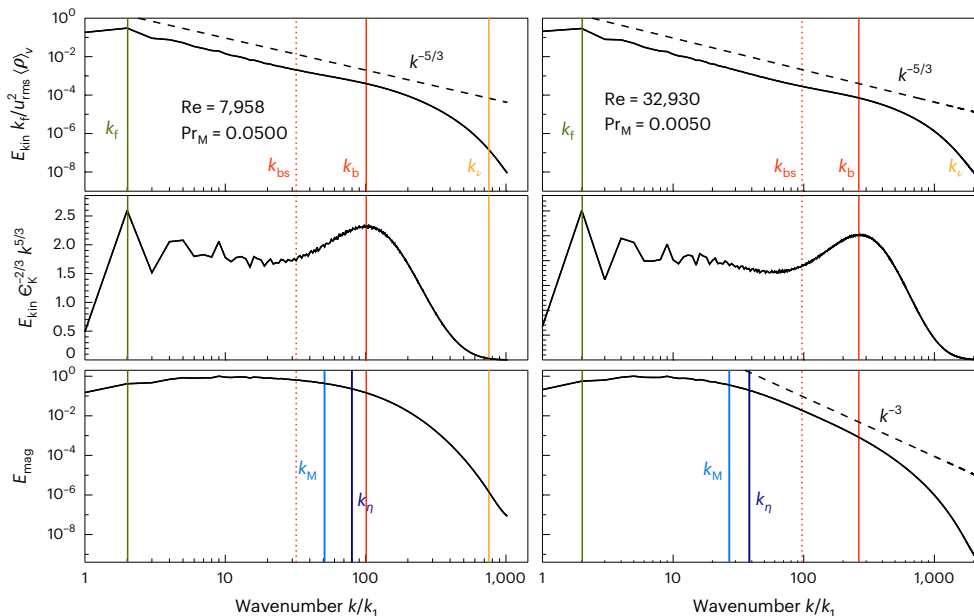

Fig. 4 | Energy spectra. Kinetic (top) and magnetic (bottom) energy spectra for two exemplary runs with Re = 7,958 and $Pr_M = 0.05$ (left), and Re = 32,930 and $Pr_M = 0.005$ (right). In the middle row, the kinetic spectra are compensated by $k^{5/3}$. Vertical lines indicate the forcing wavenumber k_f (green solid), the wavenumber of the bottleneck's peak k_b (red solid) and its starting point k_{bs} (red dotted), the

viscous dissipation wavenumber k_v (orange), the ohmic dissipation wavenumber $k_\eta = k_v Pr_M^{3/4}$ (dark blue) and the characteristic magnetic wavenumber k_M (light blue). All spectra are averaged over the kinematic phase whereupon each individual magnetic spectrum was normalized by its maximum, thus taking out the exponential growth.

highest Pr_M either, which could be an indication of an outer-scale driven SSD, as postulated by ref. [7]. Furthermore, we find that the pre-factor of $\gamma \propto \ln(Re_M/Re_M^{crit})$ is nearly constant with its mean around 0.022, in agreement with 0.023 of ref. [10]. A constant value means that the logarithmic scaling is independent of Pr_M and seems to be of general validity.

Third, we find that the measured characteristic magnetic wavenumber k_M is always smaller than the estimated k_η, and furthermore, k_M does not always follow the theory-predicted scaling of $k_\eta \propto Pr_M^{3/4}$ with Pr_M. For region I, where Pr_M is close to 1, this discrepancy is up to a factor of three and the deviation from the expected Pr_M scaling is most pronounced here. These discrepancies have been associated with the numerical set-ups injecting energy at a forcing scale far larger than the

dissipation scale, that is $k_f \ll k_\eta$ (ref. [1]). Furthermore, our runs in region I also have relatively low Re and therefore numerical effects are not dismissible. In region III (low Pr_M), k_M/k_η is approaching the constant offset factor 0.75. Hence, the scaling of k_M/k_η with Pr_M gets close to the expected one. This result again indicates that the SSD at low Pr_M is different from that at $Pr_M \approx 1$.

An increase of Re_M^{crit} with decreasing Pr_M followed by an asymptotic levelling-off for $Pr_M \ll 1$ was expected in the light of theory and previous numerical studies. Instead, we found non-monotonic behaviour as function of Pr_M; we could relate it to the hydrodynamical phenomenon of the bottleneck. If the characteristic magnetic wavenumber lies in the positive-gradient part of the compensated spectrum, where the spectral slope is markedly reduced from −5/3 to about −1.4, the dynamo
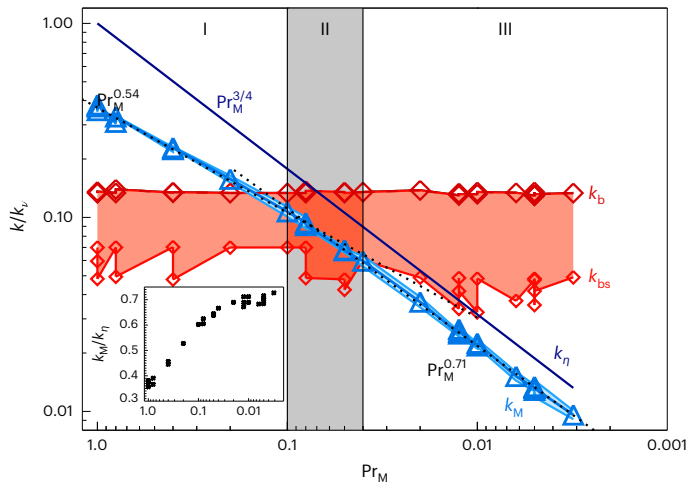
Fig. 5 | Relation of the characteristic magnetic wavenumber k_M to the bottleneck. We show its peak k_b and its starting point k_{bs} in red, the characteristic magnetic wavenumber k_M in light blue and the ohmic dissipation wavenumber k_η in dark blue. The red shaded area between k_b and k_{bs} corresponds to the low-wavenumber part of the bottleneck where the turbulent flow is rougher than for a $-5/3$ power law. The Roman numbers indicate the three distinct regions of dynamo excitation. The region of the weakest growth (II) is over-plotted in grey. The characteristic magnetic wavenumber k_M can be fitted by two power laws (black dotted lines): $k_M/k_\nu \propto Pr_M^{0.54}$ for $Pr_M \geq 0.05$ and $k_M/k_\nu \propto Pr_M^{0.71}$ for $Pr_M \leq 0.05$. All wavenumbers are normalized by the viscous one k_ν. We find that the dynamo is hardest to excite if k_M lies within the low-wavenumber side of the bottleneck. Leaving this region towards lower or higher wavenumbers makes the dynamo easier to excite. The inset shows k_M/k_η as a function of Pr_M.

is hardest to excite ($0.1 \geq Pr_M \geq 0.04$). For higher or lower Pr_M, the dynamo becomes increasingly easier to excite. The local change in slope due to the bottleneck has often been related to an increase of the 'roughness' of the flow[1,10,43], which is expected to harden dynamo excitation based on theoretical predictions[4,9] from kinematic Kazantsev theory[45]. In line with theory, the roughness-increasing part of the bottleneck appears decisive in our results, however, only when k_M is used as a criterion. The usage of k_η would in contrast suggest that the peak of the bottleneck is decisive[10]. Such interpretation appears incorrect, as the rough estimate of k_η employed here does not represent the magnetic spectrum adequately and the peak of the bottleneck does not coincide with the maximum of 'roughness'.

Methods

Numerical set-up
For our simulations, we use a cubic Cartesian box with edge length L and solve the isothermal magnetohydrodynamic equations without gravity, similar to refs. 5,47.

$$\frac{D\mathbf{u}}{Dt} = -c_s^2 \nabla \ln \rho + \mathbf{J} \times \mathbf{B}/\rho + \nabla \cdot (2\rho\nu S)/\rho + \mathbf{f}, \quad (1)$$

$$\frac{\partial \mathbf{A}}{\partial t} = \mathbf{u} \times \mathbf{B} + \eta \nabla^2 \mathbf{A}, \quad (2)$$

$$\frac{D\rho}{Dt} = -\nabla \cdot (\rho \mathbf{u}), \quad (3)$$

where $\mathbf{u}$ is the flow speed, c_s is the sound speed, ρ is the mass density, $\mathbf{B} = \nabla \times \mathbf{A}$ is the magnetic field with $\mathbf{A}$ being the vector potential and ∇ is the gradient vector. $\mathbf{J} = \nabla \times \mathbf{B}/\mu_0$ is the current density with magnetic vacuum permeability μ_0, while ν and η are constant kinematic viscosity

and magnetic diffusivity, respectively. The rate-of-strain tensor $S_{ij} = (u_{i,j} + u_{j,i})/2 - \delta_{ij}\nabla \cdot \mathbf{u}/3$ is traceless, where δ_{ij} denotes the Kronecker delta, and the Einstein notation convection applying to their indices i and j. The forcing function $\mathbf{f}$ provides random white-in-time non-helical transversal plane waves, which are added in each time step to the momentum equation (see ref. 5 for details). The wavenumbers of the forcing lie in a narrow band around $k_f = 2k_1$ with $k_1 = 2\pi/L$. Its amplitude is chosen such that the Mach number Ma $= u_{rms}/c_s$ is always around 0.082, where $u_{rms} = \sqrt{\langle \mathbf{u}^2 \rangle_V}$ is the volume and time-averaged root-mean-square value. The Ma values of all runs are listed in Supplementary Table 1. To normalize the growth rate λ, we use an estimated turnover time $\tau = 1/(u_{rms}k_f) \approx 6/(k_1 c_s)$. The boundary conditions are periodic for all quantities and we initialize the magnetic field with weak Gaussian noise.

Diffusion is controlled by the prescribed parameters ν and η. Accordingly, we define the fluid and magnetic Reynolds numbers with the forcing wavenumber k_f as

$$\text{Re} = u_{rms}/\nu k_f, \quad \text{Re}_M = u_{rms}/\eta k_f. \quad (4)$$

We performed numerical free decay experiments (Supplementary Section 7), from which we confirm that the numerical diffusivities are negligible.

The spectral kinetic and magnetic energy densities are defined via

$$\int_k E_{kin}(k)\,dk = u_{rms}^2 \langle \rho \rangle_V/2, \quad (5)$$

$$\int_k E_{mag}(k)\,dk = B_{rms}^2/2\mu_0, \quad (6)$$

where $B_{rms} = \sqrt{\langle \mathbf{B}^2 \rangle_V}$ is the volume-averaged root-mean-square value and $\langle \rho \rangle_V$ is the volume-averaged density.

Our numerical set-up employs a markedly simplified model of turbulence compared with the actual one in the Sun. There, turbulence is driven by stratified rotating convection being of course neither isothermal nor isotropic. However, these simplifications were so far necessary when performing a parameter study at such high resolutions as we do. Nevertheless, we can connect our study to solar parameters in terms of Pr_M and Ma. Their chosen values best represent the weakly stratified layers within the bulk of the solar convection zone, where $Pr_M \ll 1$ and Ma $\ll 1$. The anisotropy in the flow on small scales is much weaker there than near the surface and therefore close to our simplified set-up.

Data availability
Data for reproducing Figs. 2, 3 and 5 are included in the article and its Supplementary Information files. The raw data (time series, spectra, slices and snapshots) are provided through IDA/Fairdata service hosted at CSC, Finland, under https://doi.org/10.23729/206af669-07fd-4a30-9968-b4ded5003014. From the raw data, Figs. 1 and 4 can be reproduced.

Code availability
We use the Pencil Code[48] to perform all simulations, with parallelized fast-Fourier-transforms to calculate the spectra on the fly[49]. Pencil Code is freely available at https://github.com/pencil-code/.

References
1. Brandenburg, A. & Subramanian, K. Astrophysical magnetic fields and nonlinear dynamo theory. *Phys. Rep.* **417**, 1–209 (2005).
2. Charbonneau, P. Dynamo models of the solar cycle. *Living Rev. Sol. Phys.* **17**, 4 (2020).
3. Childress, S. & Gilbert, A. D. *Stretch, Twist, Fold: The Fast Dynamo* Lecture Notes in Physics Monographs Vol. 37 (Springer, 1995).

4. Boldyrev, S. & Cattaneo, F. Magnetic-field generation in Kolmogorov turbulence. *Phys. Rev. Lett.* **92**, 144501 (2004).

5. Haugen, N. E. L. & Brandenburg, A. Suppression of small scale dynamo action by an imposed magnetic field. *Phys. Rev. E* **70**, 036408 (2004).

6. Schekochihin, A. A., Cowley, S. C., Maron, J. L. & McWilliams, J. C. Critical magnetic Prandtl number for small-scale dynamo. *Phys. Rev. Lett.* **92**, 054502 (2004).

7. Schekochihin, A. A. et al. Fluctuation dynamo and turbulent induction at low magnetic Prandtl numbers. *New J. Phys.* **9**, 300 (2007).

8. Iskakov, A. B., Schekochihin, A. A., Cowley, S. C., McWilliams, J. C. & Proctor, M. R. E. Numerical demonstration of fluctuation dynamo at low magnetic Prandtl numbers. *Phys. Rev. Lett.* **98**, 208501 (2007).

9. Schober, J., Schleicher, D., Bovino, S. & Klessen, R. S. Small-scale dynamo at low magnetic Prandtl numbers. *Phys. Rev. E* **86**, 066412 (2012).

10. Brandenburg, A., Haugen, N. E. L., Li, X.-Y. & Subramanian, K. Varying the forcing scale in low Prandtl number dynamos. *Mon. Not. R. Astron. Soc.* **479**, 2827–2833 (2018).

11. Stix, M. *The Sun: An Introduction* (Springer, 2002).

12. Cattaneo, F. On the origin of magnetic fields in the quiet photosphere. *Astrophys. J.* **515**, 39–42 (1999).

13. Vögler, A. & Schüssler, M. A solar surface dynamo. *Astron. Astrophys.* **465**, L43–L46 (2007).

14. Kitiashvili, I. N., Kosovichev, A. G., Mansour, N. N. & Wray, A. A. Realistic modeling of local dynamo processes on the Sun. *Astrophys. J.* **809**, 84 (2015).

15. Hotta, H., Rempel, M. & Yokoyama, T. Efficient small-scale dynamo in the solar convection zone. *Astrophys. J.* **803**, 42 (2015).

16. Rempel, M. Numerical simulations of quiet Sun magnetism: on the contribution from a small-scale dynamo. *Astrophys. J.* **789**, 132 (2014).

17. Rempel, M. Small-scale dynamo simulations: magnetic field amplification in exploding granules and the role of deep and shallow recirculation. *Astrophys. J.* **859**, 161 (2018).

18. Riva, F. & Steiner, O. Methodology for estimating the magnetic Prandtl number and application to solar surface small-scale dynamo simulations. *Astron. Astrophys.* **660**, A115 (2022).

19. Käpylä, P. J., Käpylä, M. J., Olspert, N., Warnecke, J. & Brandenburg, A. Convection-driven spherical shell dynamos at varying Prandtl numbers. *Astron. Astrophys.* **599**, A4 (2017).

20. Hotta, H. & Kusano, K. Solar differential rotation reproduced with high-resolution simulation. *Nat. Astron.* **5**, 1100–1102 (2021).

21. Tobias, S. M. & Cattaneo, F. Shear-driven dynamo waves at high magnetic Reynolds number. *Nature* **497**, 463–465 (2013).

22. Bhat, P., Subramanian, K. & Brandenburg, A. A unified large/small-scale dynamo in helical turbulence. *Mon. Not. R. Astron. Soc.* **461**, 240–247 (2016).

23. Squire, J. & Bhattacharjee, A. The magnetic shear-current effect: generation of large-scale magnetic fields by the small-scale dynamo. *J. Plasma Phys.* **82**, 535820201 (2016).

24. Hotta, H., Rempel, M. & Yokoyama, T. Large-scale magnetic fields at high Reynolds numbers in magnetohydrodynamic simulations. *Science* **351**, 1427–1430 (2016).

25. Väisälä, M. S. et al. Interaction of large- and small-scale dynamos in isotropic turbulent flows from GPU-accelerated simulations. *Astrophys. J.* **907**, 83 (2021).

26. Rempel, M. Extension of the MURaM radiative MHD code for coronal simulations. *Astrophys. J.* **834**, 10 (2017).

27. Kleint, L., Berdyugina, S. V., Shapiro, A. I. & Bianda, M. Solar turbulent magnetic fields: surprisingly homogeneous distribution during the solar minimum. *Astron. Astrophys.* **524**, A37 (2010).

28. Buehler, D., Lagg, A. & Solanki, S. K. Quiet Sun magnetic fields observed by Hinode: support for a local dynamo. *Astron. Astrophys.* **555**, A33 (2013).

29. Lites, B. W., Centeno, R. & McIntosh, S. W. The solar cycle dependence of the weak internetwork flux. *Publ. Astron. Soc. Jpn* **66**, S4 (2014).

30. Bellot Rubio, L. & Orozco Suárez, D. Quiet Sun magnetic fields: an observational view. *Living Rev. Sol. Phys.* **16**, 1 (2019).

31. Faurobert, M. & Ricort, G. Magnetic flux structuring of the quiet Sun internetwork. Center-to-limb analysis of solar-cycle variations. *Astron. Astrophys.* **651**, A21 (2021).

32. Korpi-Lagg, M. J., Korpi-Lagg, A., Olspert, N. & Truong, H.-L. Solar-cycle variation of quiet-sun magnetism and surface gravity oscillation mode. *Astron. Astrophys.* **665**, A141 (2022).

33. Tobias, S. M. The turbulent dynamo. *J. Fluid Mech.* **912**, 1 (2021).

34. Schekochihin, A. A. et al. The onset of a small-scale turbulent dynamo at low magnetic Prandtl numbers. *Astrophys. J.* **625**, 115–118 (2005).

35. Tobias, S. M., Cattaneo, F. & Boldyrev, S. in *Ten Chapters in Turbulence* (eds Davidson, P. A. et al.) 351–404 (Cambridge Univ. Press, 2012); https://doi.org/10.1017/CBO9781139032810.010

36. Rogachevskii, I. & Kleeorin, N. Intermittency and anomalous scaling for magnetic fluctuations. *Phys. Rev. E* **56**, 417–426 (1997).

37. Kleeorin, N. & Rogachevskii, I. Growth rate of small-scale dynamo at low magnetic Prandtl numbers. *Phys. Scr.* **86**, 018404 (2012).

38. Falkovich, G. Bottleneck phenomenon in developed turbulence. *Phys. Fluids* **6**, 1411–1414 (1994).

39. Lohse, D. & Müller-Groeling, A. Bottleneck effects in turbulence: scaling phenomena in *r* versus *p* space. *Phys. Rev. Lett.* **74**, 1747–1750 (1995).

40. She, Z.-S. & Jackson, E. On the universal form of energy spectra in fully developed turbulence. *Phys. Fluids A* **5**, 1526–1528 (1993).

41. Saddoughi, S. G. & Veeravalli, S. V. Local isotropy in turbulent boundary layers at high Reynolds number. *J. Fluid Mech.* **268**, 333–372 (1994).

42. Küchler, C., Bewley, G. & Bodenschatz, E. Experimental study of the bottleneck in fully developed turbulence. *J. Stat. Phys.* **175**, 617–639 (2019).

43. Dobler, W., Haugen, N. E., Yousef, T. A. & Brandenburg, A. Bottleneck effect in three-dimensional turbulence simulations. *Phys. Rev. E* **68**, 026304 (2003).

44. Donzis, D. A. & Sreenivasan, K. R. The bottleneck effect and the Kolmogorov constant in isotropic turbulence. *J. Fluid Mech.* **657**, 171–188 (2010).

45. Kazantsev, A. P. Enhancement of a magnetic field by a conducting fluid. *Sov. J. Exp. Theor. Phys.* **26**, 1031 (1968).

46. Brandenburg, A. Nonlinear small-scale dynamos at low magnetic Prandtl numbers. *Astrophys. J.* **741**, 92 (2011).

47. Brandenburg, A. The inverse cascade and nonlinear alpha-effect in simulations of isotropic helical hydromagnetic turbulence. *Astrophys. J.* **550**, 824–840 (2001).

48. Pencil Code Collaboration et al. The Pencil Code, a modular MPI code for partial differential equations and particles: multipurpose and multiuser-maintained. *J. Open Source Softw.* **6**, 2807 (2021).

49. Bourdin, P.-A. Driving solar coronal MHD simulations on high-performance computers. *Geophys. Astrophys. Fluid Dyn.* **114**, 235–260 (2020).

Acknowledgements

Author contributions

J.W. led and all the authors contributed to the design and performing the numerical simulations. J.W. led the data analysis. M.J.K.-L. was in charge of acquiring the computational resources from CSC. All the authors contributed to the interpretation of the results and writing the paper.

Competing interests

The authors declare no competing interests.

Additional information

Supplementary information The online version contains supplementary material available at https://doi.org/10.1038/s41550-023-01975-1.

Correspondence and requests for materials should be addressed to Jörn Warnecke.

Reprints and permissions information is available at www.nature.com/reprints.

Publisher's note Springer Nature remains neutral with regard to jurisdictional claims in published maps and institutional affiliations.